I&EC research
Industrial & Engineering Chemistry Research

ARTICLE

pubs.acs.org/IECR

Texture-Based Foam Segmentation and Analysis

Wei Wang,[†] Xiaolei Huang,[*,†] and Ali Esmaili[*,‡]

[†]Department of Computer Science and Engineering, Lehigh University, Bethlehem, Pennsylvania 18015, United States

[‡]Process Data Technology, Air Products and Chemicals, Inc., Allentown, Pennsylvania 18195, United States

ABSTRACT: A variety of polymers or surfactant mixtures or aeration of a number of liquids could generate mixtures of liquid and foam. Therefore, characterizing the properties of liquid/foam mixtures has important applications in the chemical process industry. The lack of a robust automated method for characterization within limited time and with high accuracy, however, has made this task difficult. In this work, we propose a new method based on image analysis for quantifying the geometric and statistical properties of such liquid/foam mixtures using images captured by an optical camera. The method can reliably achieve automated segmentation of liquid and foam layers. It can also find the boundaries of individual bubbles in the foam layer. At first, the region of interest, the foam region, is segmented from the input raw image. Then, the foam region is partitioned into two types of subregions, namely, loose foam or dense foam, according to local texture feature analysis. In the next step, to segment bubbles within the foam to obtain quantitative characterization, we apply two image processing algorithms, namely, Canny edge detection and K-means clustering, each specific to a different type of foam (loose or dense). The results show that the proposed automated segmentation and characterization method is robust and applicable to the processing of foam/liquid mixtures under many conditions.

1. INTRODUCTION

Characterization of foam/liquid mixtures is important, because mixture properties can provide insight into the underlying chemical properties and other attributes. Many studies performed in the past several decades[1−5] have focused on how to achieve and maintain desired foam properties such as foam texture, foam viscosity, and solid-carrying capability. For instance, in waterborne paints and coatings,[4−6] foams can cause surface irregularities, reduce gloss and transparency, and adversely affect the protective properties of coatings. Thus, effective defoamers or deaerators are sought to break down foam and release entrained air. In the petroleum industry,[7] foams can be used as a lightweight drilling fluid in underbalanced drilling applications. Drilling with foam has been shown to provide significant benefits including increased drilling rate, minimization of lost circulation, reduction of differential pipe sticking, and reduced formation damage. Foams are also used in a large variety of other industrial applications:[8−10] liquid foams are employed to separate minerals from extracted ore in the process of flotation, foams are used as fire-fighting agents for polar solvent and oil fires, and foams are encountered in many food products and cosmetics in everyday life.

Foam analysis has traditionally been performed in a manual manner in different domains of study.[11,12] However, manual measurement of some foam and liquid properties can be time-consuming, and certain important geometric and dynamic measures are difficult or impossible to quantify using manual methods. The challenges in foam analysis are comprehensively described in ref 13. In recent years, advanced imaging equipment has become readily available at reasonable prices, which opens opportunities for new methods to be devised to perform image analysis on foam and liquid mixtures and to achieve quantification of important foam properties through parameters extracted from image information. Typically some of the variables that can be quantified are derived from geometric and color parameters. For instance, bubble size distribution indicates foam texture, bubble rising velocity reflects viscosity, transmittance reveals color/intensity and transparency, and contact angles at liquid−air and liquid−solid interfaces can be used to infer information about surface tension.

Some previous automated or semiautomated methods of image-based foam analysis have been proposed to characterize properties of foams that vary from solid to liquid, such as the froth flotation of coal,[14] metal foams,[15] foams in beer,[16] and protein/surfactant foams.[17] For three-dimensional foams, tomographic measurement methods[18] have been reported, but the use of X-ray tomography tends to increase the cost of experimentation. Several image-based methods[19−22] have been proposed for measuring particle properties. These methods can have difficulty detecting densely dispersed particles, because, in images of dense foam, two or more overlapping particles are prone to being erroneously detected as one larger particle using approaches that track either the boundary contour or the pixel cluster of a particle.[19] A template-based detection method[21] was proposed for analyzing images captured by a single optical camera. Although this approach was found to be more successful in characterizing dense/wet foams when compared with previous tomographic methods, it considers only roughly spherical particles, and its results depend on the similarity (or uniformity) of the bubbles within the foam. In another approach,[22] active contour models (or "snakes"),[23] which are physically based energy-minimizing spline curves, are applied to extract the boundaries of sparsely dispersed single particles. This approach can produce precise geometric measurements, but it requires manual initialization for each particle, which makes it unsuitable

Received: August 25, 2010
Accepted: March 8, 2011
Revised: March 7, 2011
Published: April 05, 2011

dx.doi.org/10.1021/ie1017833 | *Ind. Eng. Chem. Res.* 2011, 50, 6071–6081

for characterizing dense foams. In a recent work,[20] a method based on watershed transform[24] was proposed to segment and track foam bubbles. However, it is still challenging for this method to detect dense foam bubbles, as the values for a required parameter of the method, the regional intensity maxima, are difficult to obtain in dense foam regions because of image noise. The high computational cost is another problem with using watershed-transform-based methods, but it could be addressed using parallel implementations.[25]

In this work, we develop a novel image-based approach for automatically extracting useful liquid/foam mixture properties. The foam and liquid mixtures with which we worked were produced in a study of defoaming theory and applications in paints and coatings. To evaluate the potential of different chemical mixtures for paints and coatings and compare the properties of various defoamers, we aim to develop an efficient and robust method for automatically extracting some of the following foam and liquid parameters: bubble size distribution, color and transmittance, contact angles at interfaces, and bubble rising velocity. These parameters will enable the quantitative measurement of important mixture properties such as foam density, viscosity, and surface tension.

Our approach uses image analysis algorithms to reliably segment foam and liquid regions in a mixture and derives a host of important geometric and optical parameters. We analyze foam texture using an entropy-based method that can differentiate between dense and loose foam types. Then, image analysis pipelines specific to each foam type are subsequently devised to achieve segmentation of bubbles in the foam. Geometric parameters such as the centroid and diameter of each bubble and heights of the liquid and foam layers, are extracted by applying morphological operations (or blob analysis) to the segmented result. Finally, optical properties such as color transmittance are estimated by fitting a polynomial surface to the background colors and then comparing the background with foreground colors in the segmented foam/liquid regions. In our experiments, this approach achieved consistent performance on a variety of foams: the foams that were successfully characterized were made of densely packed small bubbles, sparsely dispersed large bubbles, or a mixture of the two types. Furthermore, because our approach relies on computer analysis to extract meaningful data from foam/liquid images that can be captured quickly and conveniently using optical cameras, it is very useful for high-throughput characterization of mixture properties in industrial laboratories.

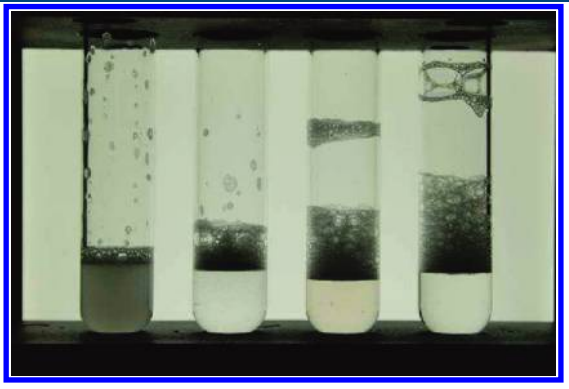

Figure 1. Sample raw image.

2. MATERIALS AND METHODS

The test data for this work consisted of over 1000 high-resolution (3888 × 2952 pixels) optical images, taken with a digital camera in a stable laboratory environment. A typical sample raw image is shown in Figure 1. The ISO sensitivity value and focal length of the camera were 100 and 55 mm, respectively. Other important camera parameters such as the shutter speed, aperture, and distance to the object were varied, and the optimal settings (shutter speed, 0.04 s; aperture, F/10; object distance, 57.15 cm) were chosen according to performance measures in an edge-detection benchmark task. In the benchmark task, the Sobel edge detector was applied on 100 raw images that were taken using a variety of camera settings. [The Sobel edge detector was used in the benchmark task because it is efficient and does not have any parameter for its computation.] We visually examined the edge output of each image and rated the quality of the detected edges by giving a score ranging from 1 (poor) to 5 (good). For instance, if all edges of interest (e.g., tube edges, foam/liquid layer boundary, most bubble edges) were detected, we gave a high score; if some important edges were missing, we gave a low score. We calculated the average edge-quality score for images taken with the same camera setting and chose the setting with the highest average score as the optimal camera setting. In the complete set of over 1000 raw images, 340 images were taken with the camera at the chosen optimal setting, and we used these 340 images to test our foam segmentation and characterization algorithms.

The overall flow diagram for our system of using images to characterize foam and liquid properties is presented in Figure 2. Given an input raw image, as shown in Figure 1, our system first automatically segments the regions of interest, which include foam and liquid layers. The segmentation of foam and liquid regions from the raw image is achieved using the Canny edge detection[26] method in several steps: (1) delineation of the tube rack boundary, (2) segmentation of test tubes within the rack area, and (3) segmentation of foam and liquid layers within each test tube. The system then analyzes the segmented foam layers. It classifies two different kinds of foam, namely, loose foam and dense foam, according to local texture features. To segment bubbles within the foam, Canny edge detection is used again to segment large bubbles in loose foam regions, whereas K-means clustering[27] is applied to segment bubbles in dense foam regions.

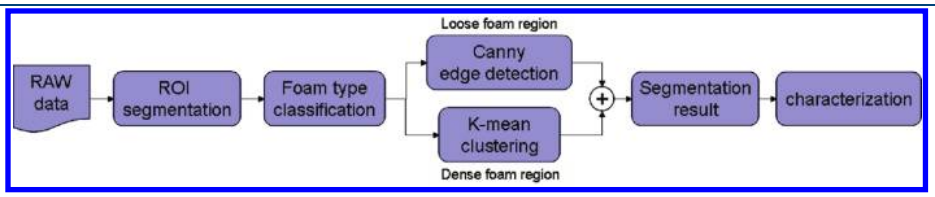

Figure 2. Overall flow diagram for the image-based foam and liquid characterization system.

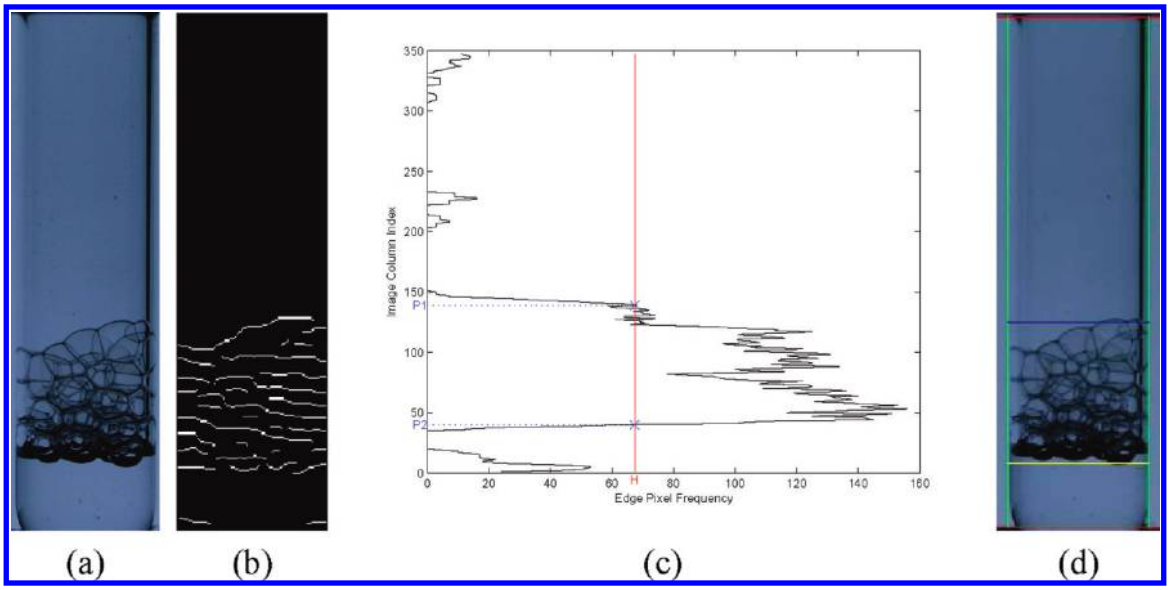

Figure 3. Foam layer segmentation: (a) Original tube segment, (b) Canny edge map, (c) plot of edge-pixel count in each row, (d) foam layer segmentation result.

After these segmentation steps, we extract key parameters for characterization of the bubble diameter and density, as well as the color transmittance values of the liquid and foam regions. Next, we describe each step in the system in detail.

2.1. Foam Layer Segmentation. In the 340 images selected for our test set, some images included only liquid, whereas others included liquid and foam. We used Canny edge detection[26] and two-dimensional characterization of the edge maps to recognize and segment foam layers with high accuracy.

The Canny edge detector is a widely used method for detecting edges in images. It first applies Gaussian smoothing to reduce noise in the image. Then, the image gradient is computed, and areas of the image with high gradient magnitudes (above a threshold) are identified. A nonmaximum suppression step tests each pixel in the high-gradient-magnitude region and further suppresses those pixels that do not have the local maximum gradient magnitude along the gradient direction. Finally, hysteresis is used to connect the remaining pixels that have not been suppressed. Hysteresis uses two thresholds: If a pixel's gradient magnitude is below the lower threshold, its edge map output value is set to 0 (i.e., a nonedge pixel). If the magnitude is above the higher threshold, its edge map output value is set to 1 (i.e., an edge pixel). If the magnitude lies in between the two thresholds, the pixel is considered an edge pixel only if it is connected to another pixel that is known to be an edge pixel.

In our system, the Canny edge detection algorithm is applied to delineate the boundaries of the tube rack and individual test tubes, as well as the boundaries between foam and liquid layers. (It is used again later, in subsection 2.3.1, for detecting bubble boundaries in loosely packed foam regions.) Figure 3 illustrates the process of foam layer segmentation. On a segmented tube region (Figure 3a), the result of Canny edge detection is shown in Figure 3b. Because the test tube hold ing the foam and liquid mixture is kept in an upright position by the rack, we count the number of edge pixels along each pixel row, and plot a one-dimensional profile of edge-pixel count. Such a plot can be seen in Figure 3c, where the vertical Y axis represents the row (or Y) index of the image and the horizontal X axis represents edge-pixel count (i.e., total number of edge pixels) along the rows. Because there are more edges in foam regions, which corresponds to high edge-pixel counts in these regions, we detect the horizontal boundary edges of foam layers by applying a threshold, H, on the row-wise edge-pixel count value. More specifically, in Figure 3c, let P_1 and P_2 denote the row indexes of the upper and lower boundaries of the foam layer. Then, P_1 is found as the index of the first row with edge-pixel count value greater than the threshold H, and P_2 is the index of the last row that satisfies the same condition. The threshold value H is usually set as the number of pixels, along a single row, required to cover half of the tube width. In Figure 3d, two horizontal lines are drawn to mark the detected upper and lower boundaries of the foam layer.

2.2. Foam Type Classification. Because of large variations in the size and shape of foam bubbles, we define two different types of foam according to local texture features and apply a different bubble segmentation method to each type. In this subsection, we introduce the algorithm for foam type classification, and then in subsection 2.3, we introduce the bubble segmentation methods.

2.2.1. Local Texture Features. In many machine vision and image processing algorithms, simplifying assumptions are made about the uniformity of the intensity in local image regions. However, images of real objects often do not exhibit regions of uniform intensity. For instance, foam bubbles form distinctive texture patterns, and the intensity within a foam region is not uniform because of variations in foam density, illumination, reflection, and refraction. We propose a local entropy-based texture analysis method for classifying foam type according to local foam texture characteristics.

In information theory, entropy measures the uncertainty associated with a random variable.[28] Considering a local image region R (e.g., 5 × 5 window) centered at a pixel. Representing the pixel intensities in the region by a random variable I, one can compute the entropy associated with the random variable. Suppose the probability of $I = i$, $i = 0, 1, ..., 255$ (i.e., the

dx.doi.org/10.1021/ie1017833 |*Ind. Eng. Chem. Res.* 2011, 50, 6071–6081

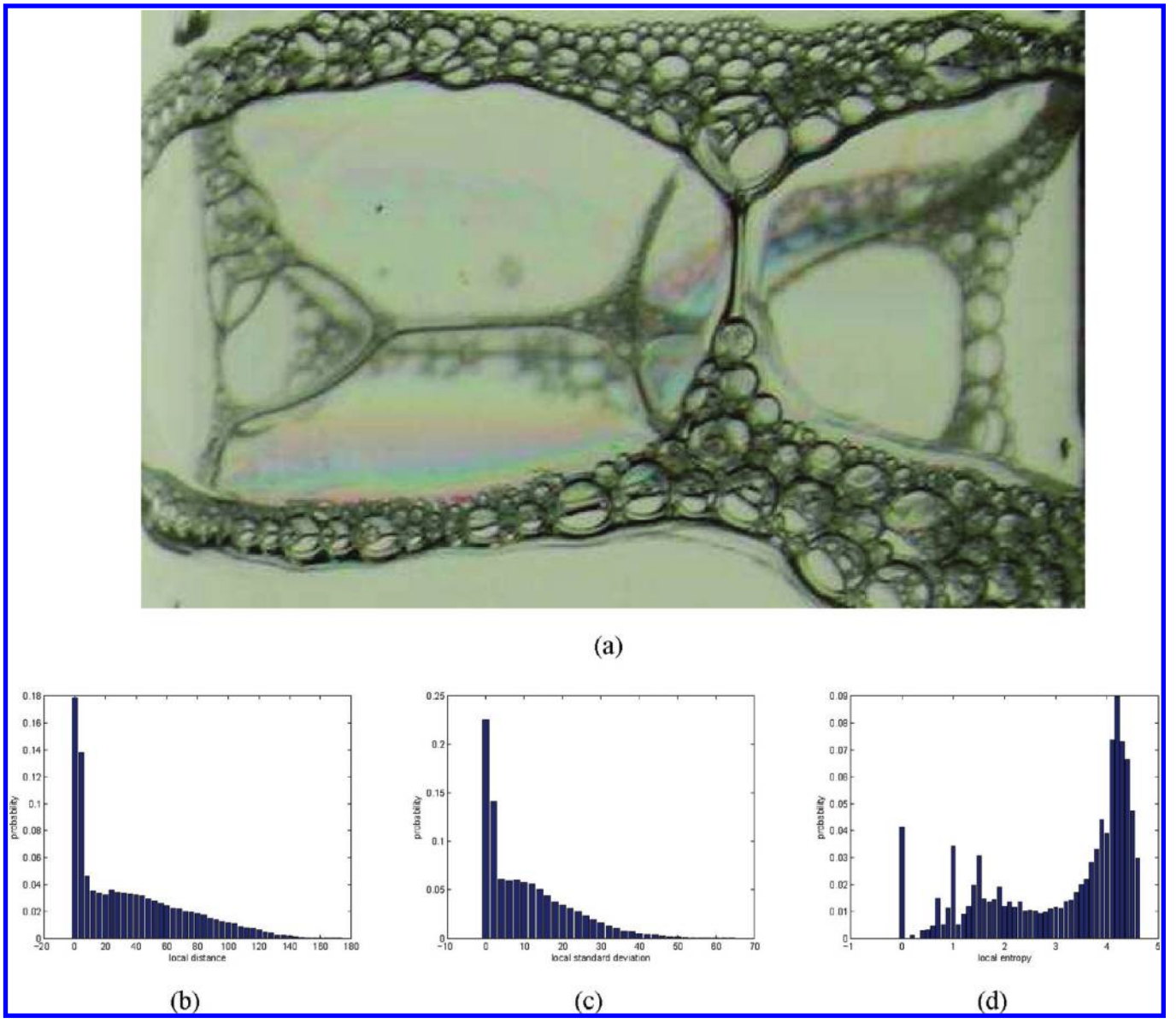

Figure 4. Comparison of the probability distributions of three local texture features in characterizing a foam layer: (a) Original foam layer image, (b) distribution of local distance (or range) values, (c) distribution of local standard deviation values, (d) distribution of local entropy values.

probability of intensity value i in region R), is $p(i)$. Then, the local entropy is defined by

$$H(I) = -\sum_i p(i) \log_2[p(i)] \quad (1)$$

From this entropy equation, one can see that the highest entropy is realized when all intensity values are equally probable. That is, a flat histogram in region R gives high entropy, whereas a peaked histogram gives low entropy. Therefore, the amount of entropy for a region indicates the level of correlation among individual pixel intensities in the region: a homogeneous region has low entropy, whereas a textured region with rich edge features has high entropy. This is the basis for utilizing local entropy for foam texture analysis.

In addition to local entropy, we also explored several other texture features, including local distance and local standard deviation. In a local region R centered at a pixel, the local distance feature is the intensity range in the region. Again denoting the intensity random variable by I and supposing the maximum and minimum intensities in the region to be i_{max} and i_{min}, respectively, the local distance is defined as

$$D(I) = i_{max} - i_{min} \quad (2)$$

Another feature, the local standard deviation, is the standard deviation of the intensity values in the local region R, defined by

$$\sigma(I) = \sqrt{\sum_i p(i)(i-\mu)^2} \quad (3)$$

where μ is the mean intensity: $\mu = \Sigma_i i p(i)$.

2.2.2. Foam Type Classification. Given a segmented foam layer, we computed the local entropy, local distance, and local standard deviation features for every pixel in the layer, using information from the local neighborhood region around that pixel. Figure 4b–d shows a comparison of the three features'

dx.doi.org/10.1021/ie1017833 |*Ind. Eng. Chem. Res.* 2011, 50, 6071–6081

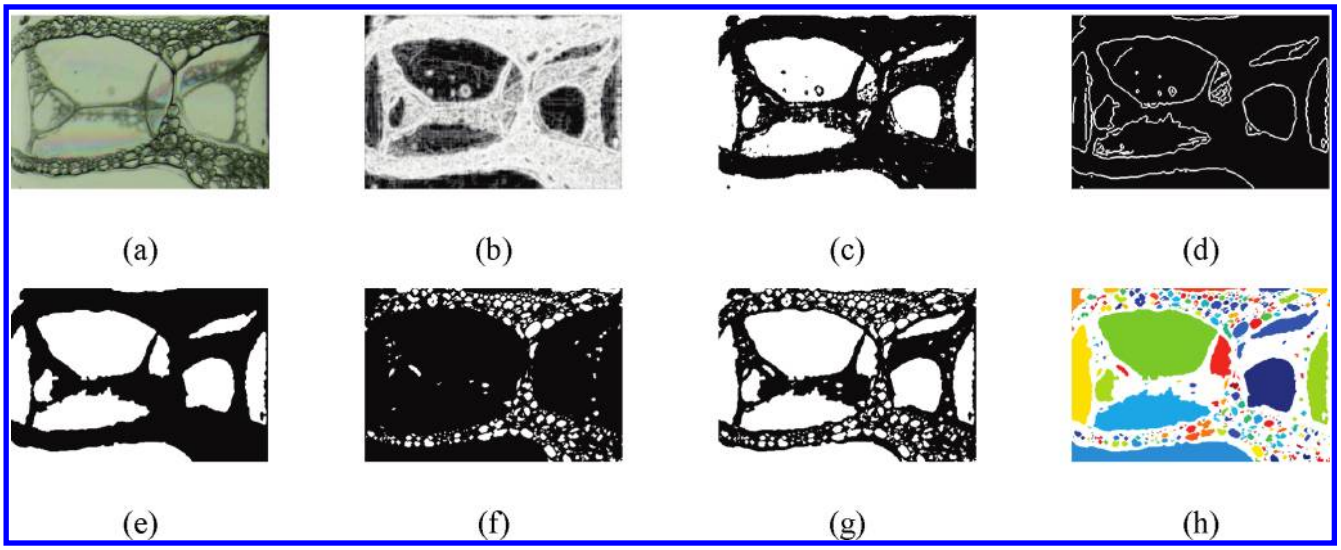

Figure 5. Foam classification and bubble segmentation: (a) Original image, (b) entropy map, (c) classified loose foam regions (white foreground) and dense foam regions (black background), (d) edge map within the loose foam regions, (e) refined segmentation of loose foam bubbles (foreground), (f) dense bubble segmentation results (foreground), (g) binary map with all bubbles as foreground, (h) bubble blobs rendered in different colors.

probability distributions for pixels in the foam layer displayed in Figure 4a. In this example, the foam layer contained two types of foam: loose foam and dense foam. Because our objective was to distinguish between pixels in dense foam and in loose foam regions, the local entropy feature provided a two-peak distribution whose two peaks represent the two types of foam. Similar patterns were observed for the local entropy feature using other images, making it well-suited for texture-based foam classification.

There has been prior work on using local entropy features for segmentation of natural[29] and medical images.[30] For analyzing chemical liquid/foam mixture images, we found that local entropy features perform better than the local distance and local standard deviation features. Therefore, we adopted a method based on local entropy features for foam type classification: A threshold was set on the local entropy feature value of a pixel. If the entropy value was above the threshold, the pixel was classified as part of a dense foam region; otherwise, it was classified as part of a loose foam region. The threshold value was selected empirically based on experimental trials on a subset of 20 randomly picked images. For the sample foam layer shown in Figure 5a, the local entropy map can be seen in Figure 5b, and the foam type classification result can be seen in Figure 5c, where the dense foam regions are black and the loose foam regions are white.

2.3. Bubble Segmentation. Within the segmented foam regions, we applied further processing to segment the individual bubbles and extract bubble boundaries to quantify foam properties such as bubble size and density. Two different bubble segmentation methods were applied to the two types of foam regions: dense and loose.

2.3.1. Bubble Segmentation in Loose Foam Regions. In loose foam regions, bubble sizes are large, and there are clear edges between neighboring bubbles. In addition, there is often a smoothly varying luminance within a single bubble, so uniform intensity within a bubble cannot be assumed. Therefore, edge detection methods that detect sharp contrast give more accurate bubble boundaries than intensity-based methods. The process started with regions classified as loose foam (e.g., white regions in Figure 5c). A morphological dilation was applied to the loose-foam regions to ensure that the enlarged regions fully covered the areas where the "loose" (or large) bubbles resided. We then used the Canny edge detector to find edge pixels in the dilated regions. The edge pixels were linked to form connected chains, which were identified as potential bubble boundaries (Figure 5d). Finally, we determined true loose bubble boundaries by simultaneously considering the connected edge chains and the loose foam regions: only closed edge chains were kept as bubble boundaries, and very short edge chains that resided inside a large loose foam region were discarded. In this way, clear and refined boundary edges of bubbles in loose foam regions were generated. The final output of this processing is a binary map with all of the segmented loose bubbles (enclosed by the detected bubble boundaries) as the foreground (Figure 5e).

2.3.2. Bubble Segmentation in Dense Foam Regions. To segment bubbles in dense foam regions, edge detection is not suitable because the cluttered small bubbles give complex and busy edges that are difficult to connect accurately to form clean bubble boundaries. Considering that the luminance is relatively constant in a single bubble in a dense foam region because of the small bubble size, we adopted the K-means clustering method[27] to achieve acceptable dense bubble segmentation results.

In our dense bubble segmentation problem, we aimed to group all of the pixels in regions classified as dense foam (e.g., the black region in Figure 5e) into two clusters: one for bubble interiors, and the other for bubble boundaries. That is, given a total of n pixels in dense foam regions, we classified each pixel as being either inside some bubble or on the boundary between bubbles, which means $k = 2$ in the K-means clustering algorithm. The data points (or attributes) used for clustering were the pixels' intensity values. In the clustering result, the cluster with brighter intensity consisted of pixels inside bubbles, and the other cluster consisted of pixels on bubble boundaries. The dense bubble segmentation result obtained in this way for Figure 5a is shown in Figure 5f.

Although the luminance in a single dense bubble is relatively constant, the K-means clustering result is sensitive to uneven illumination across the entire dense foam region. For instance,

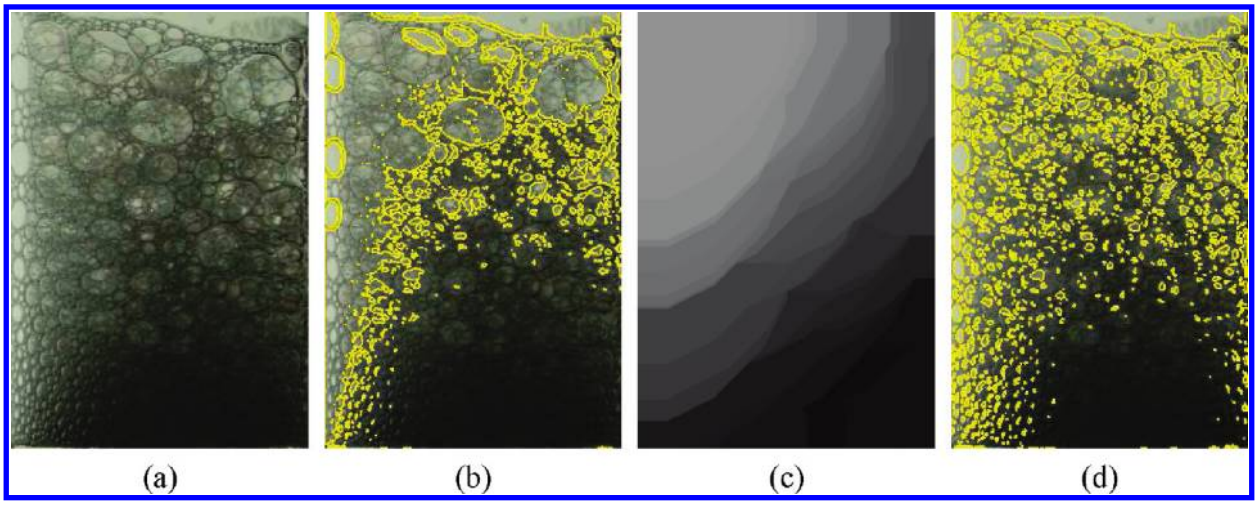

Figure 6. Sample result of dense bubble segmentation: (a) Original image, (b) segmentation result (from K-means clustering, $k = 2$) without illumination correction, (c) estimated background illumination, (d) segmentation result with illumination correction by K-means clustering on background-subtracted image.

Table 1. Parameters Used in Two-Dimensional Characterization of Bubbles in Foam

parameter	definition
centroid	center of the bubble
area	number of pixels contained within the boundary of the bubble
perimeter	number of pixels present on the boundary of the bubble
aspect ratio	maximum ratio of width to height of a bounding rectangle for the measured bubble; minimum value of 1
compactness	ratio of the area of the bubble to the square of the perimeter of the bubble; maximum value of 1
distribution of bubble diameter	distribution of bubble diameters with respect to the frequency of occurrences
distribution of bubble perimeter	distribution of bubble perimeters with respect to the frequency of occurrences
distribution of aspect ratio	distribution of bubble aspect ratios with respect to the frequency of occurrences
distribution of compactness	distribution of bubble compactness values with respect to the frequency of occurrences

Figure 6b shows two clusters of a dense foam region (Figure 6a) without any illumination correction. Here, the brighter upper area becomes one cluster, and the lower denser foam area is another cluster, making it impossible to detect and segment individual bubbles in the upper area. To address this problem, we introduced an illumination correction step before K-means clustering. The correction of illumination was achieved by subtracting from the original image an estimated background illumination map. To obtain the background illumination map, we applied a morphological open operation (i.e., an erosion followed by a dilation) on the foam image, with a flat, disk-shaped structuring element. Figure 6c shows the estimated background illumination. After subtracting the background, K-means clustering was found to give significantly better dense bubble segmentation result; see Figure 6d.

2.3.3. Two-Dimensional Characterization. In the last step, we combined the segmentation results from loose and dense foam together. The binary map with loose bubbles as foreground and the binary map with dense bubbles as foreground were merged into one binary map with all bubbles as foreground (e.g., Figure 5g). Connected component labeling and analysis[31] was then applied to group foreground pixels connected to each other. Each connected component (or blob) corresponds to a segmented bubble. In Figure 5h, each bubble blob is rendered in a different color. Now, the parameters of individual bubbles or statistics about certain parameters among all bubbles can be obtained. We selected the set of parameters listed in Table 1 to characterize the bubbles. These parameters have been shown to have an inherent relationship with the properties of the chemicals that produced the foam.[15]

3. RESULTS

We implemented our system in Matlab 2007b on a computer with an Intel Core2 E6850 CPU and 3 GB of memory. On average, less than 5 s was required to segment tubes (four tubes per image) and the liquid and foam layers within each tube. Depending on the height of the foam layer, from 0.9 to 4.1 s was required to process one foam layer, including foam classification, bubble segmentation, and complete two-dimensional characterization. Adding time to save all of the segmentation results and write the characterization output to an Excel spreadsheet, the overall processing time for an image was around 20 s. This is much faster than manual recording and visual characterization, not to mention that our automated method can provide some bubble statistics that are impossible to obtain with manual examination. The system we built is now being used routinely in an industrial laboratory setting. Next, we present more details on the tests and evaluations we conducted on our system.

3.1. Foam Layer Segmentation. First, we show an example of foam and liquid layer segmentation in Figure 7. Given the raw image, Canny edge detection was applied to first delineate the boundaries of the tube rack, as shown by the red lines in Figure 7. Within the rack area, we further segmented the tubes by Canny

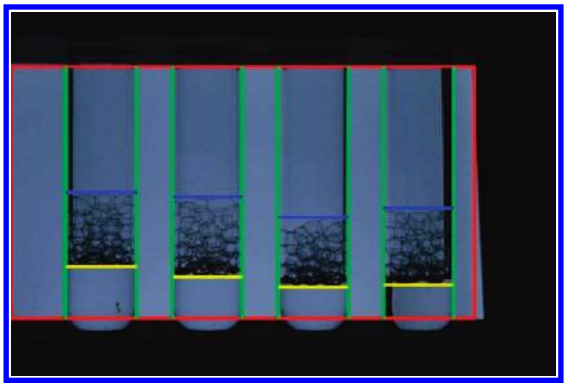

Figure 7. Foam and liquid layer segmentation in tubes. The estimated transmittance values (as defined in eq 6) of the segmented liquid layers, from left to right, are 0.9255, 0.9149, 0.9150, and 0.8557, and the transmittance values of the segmented foam layers, from left to right, are 0.6063, 0.6705, 0.6148, and 0.6054.

Table 2. Percentage of Correct Segmentations in 340 Images

region or layer	correctness (%)
rack	100
tubes	100
liquid layer	99.7
foam layer	99.3

edge detection, as shown by the green lines in Figure 7; this was achieved by locating pairs of long vertical edges. Then, within each tube, we applied the method described in subsection 2.1 to detect the upper (blue line in Figure 7) and lower (yellow line in Figure 7) boundary edges of the foam layer. Any liquid layer between the foam layer and the bottom of the rack was also segmented. We estimated the transmittance values of the segmented liquid and foam layers as shown in the explanatory text of Figure 7; the estimation method is explained later in the subsection 3.4.

To evaluate the segmentation results, we first checked the correctness by visually assessing whether the automatically detected layer edges were roughly at the correct positions. Table 2 summarizes the correctness measure of layer segmentations in the 340 images, each of which included four tubes.

To further quantitatively evaluate the accuracy of the segmentation results, we randomly selected 36 test images to obtain manual "ground truth" by manually marking the foam and liquid layer boundaries in these images. We collected such data on a total of 141 tubes with liquid, among which 63 tubes also contain foam. In this manual process, the heights of the liquid layers were found to vary from 15 to 65 mm, and those of the foam layers varied from 1.4 to 13.4 mm. To obtain quantitative accuracy measures, we compared our automated segmentation results with the manual results and recorded the mean and standard deviation of the distances between the automatically computed boundaries and their corresponding manually marked boundaries. Table 3 presents the mean and standard deviation values for the foam and liquid layers. One can see that, for both kinds of layers, the mean distance between our automatic results and the manual data was less than 0.4 mm, which is small compared to the average height of these layers.

3.2. Foam Type Classification and Bubble Segmentation. In Figure 8, we show three examples of foam classification and bubble segmentation in segmented foam layers. The original foam layer images are displayed in Figure 8a. We followed the processing steps described in subsections 2.2 and 2.3. First, texture features for every pixel in the foam layer were computed using 5×5 neighborhood windows. The computed local entropy texture map is shown in Figure 8b. For pixels near image borders, we used symmetric padding during texture computation, where the values of padding pixels were the mirror reflection of the border pixels. Using a threshold that separated the two modes of the local entropy probability density function, the classified foam regions were obtained as shown in Figure 8c, where the white regions indicate loose foam and the black regions indicate dense foam. One can see that the classification results are fairly consistent with visual examination. Next, bubbles in the loose foam regions were segmented by Canny edge detection, and bubbles in the dense foam regions were segmented using K-means clustering. The final bubble segmentation results are shown in Figure 8d, where the bubble boundaries are plotted with red lines on top of the original foam layer images.

Table 3. Statistics of the Distances between Our Automatically Computed Boundaries and the Manually Marked Boundaries of Foam and Liquid Layers in 141 Tubes

layer	mean (mm)	standard deviation (mm)
foam layer	0.3259	0.2410
liquid layer	0.3924	0.3073

Further, we compared the performance of our bubble segmentation method with the traditional watershed transform[24] and the method presented in ref 20. The method in ref 20 is based on iteratively applying the watershed transform for every possible scale of bubbles. We ran our algorithm on a test image used in ref 20. The results are shown in Figure 9. One can see that, for this image, our method (Figure 9d) outperforms the traditional watershed transform[24] (Figure 9b) and achieves a high accuracy similar to that of the method in ref 20 (Figure 9c). More comparison results between our method and the traditional watershed transform are shown in Figure 8d,e; one can see that our method gives more accurate results than the watershed method, especially in segmenting small bubbles. In terms of efficiency, our method required an average of about 2.3 s to classify foam and segment bubbles in a foam layer. The traditional (one-iteration) watershed transform takes roughly the same amount of time (about 2.1 s) to segment bubbles in a foam layer. The method in ref 20 is less efficient, especially for foams that contain bubbles with a large variety of sizes (e.g., foams shown in Figure 8), because it requires multiple iterations of the watershed transform applied in a coarse-to-fine manner.

3.3. Two-Dimensional Foam Characterization. Once the bubbles within the foam layer have been segmented, the properties of these bubbles can be measured, and two-dimensional characterization of bubble statistics can be performed. The bubble parameters that we characterized are listed in Table 1. Figure 10 shows the distributions of bubble diameter, perimeter, aspect ratio, and compactness for the foam image in Figure 9d. The bubble diameter and bubble perimeter distributions correctly reflect that there are a range of small to medium-sized bubbles, along with a few large bubbles. The facts that the weight of the aspect ratio distribution is shifted to the right and the average is above 0.5 reflect that most bubbles are not circular but have an elongated, elliptical shape.

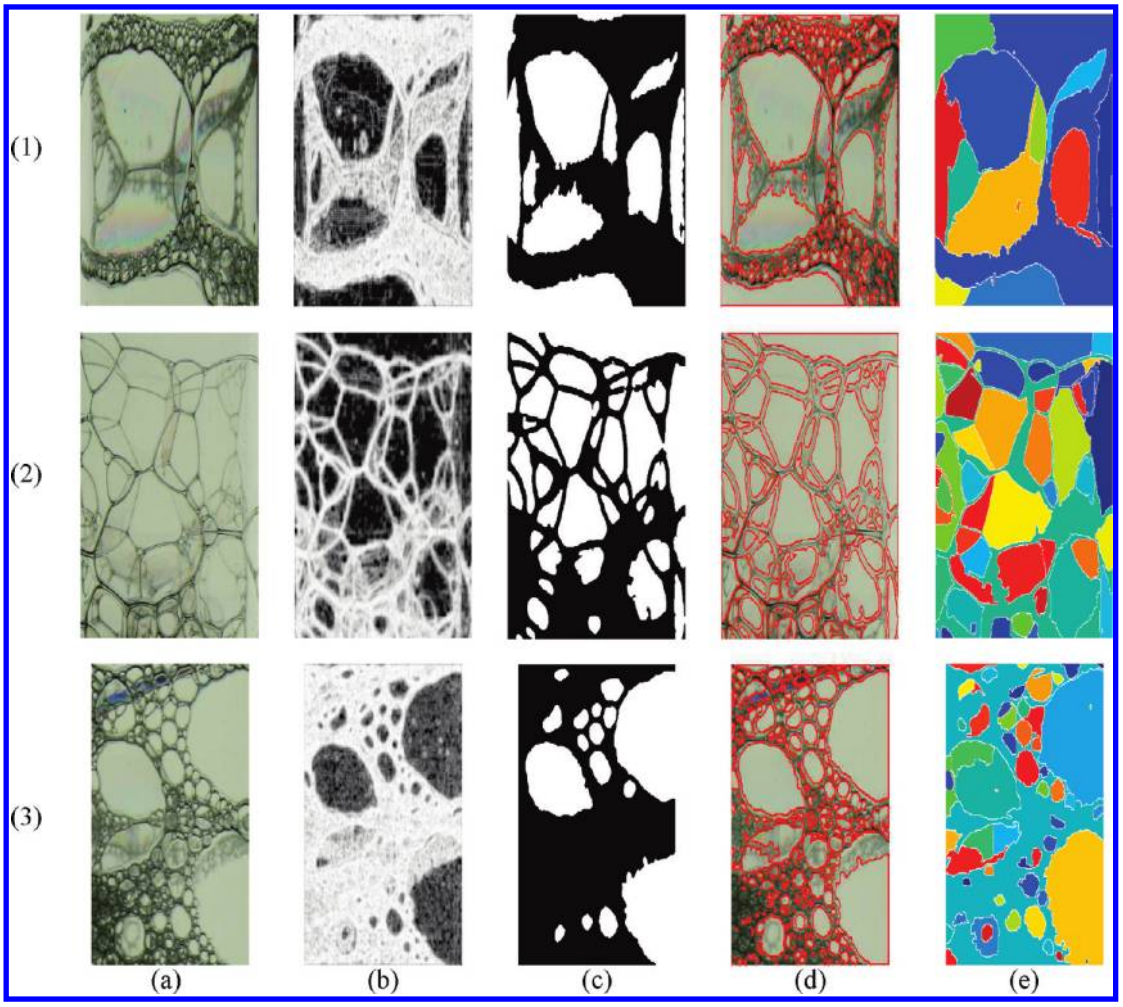

Figure 8. More results on foam classification and bubble segmentation. (a) Original images; (b) local entropy texture maps; (c) classified foam regions; (d) result from our proposed method, with bubble boundaries overlaid on original images; (e) result from traditional watershed transform.[24]

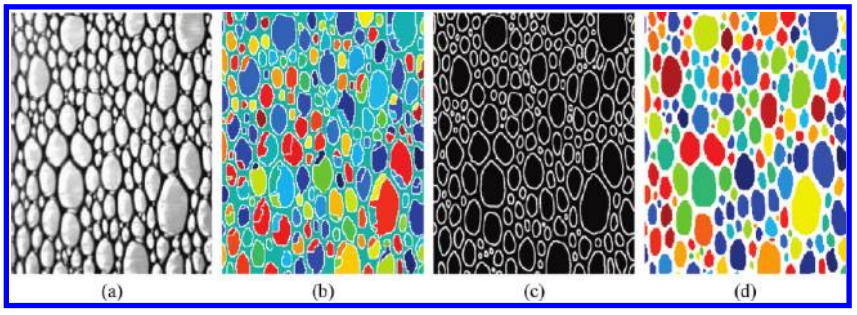

Figure 9. Comparison of bubble segmentation results: (a) Original image, (b) result from traditional watershed transform,[24] (c) result from the method presented in ref 20, (d) result from our proposed method.

3.4. Image-Based Liquid Transmittance Estimation. Within our framework, one can also automatically estimate the transmittance of liquid layers based on image information. According to the Lambert−Beer law, the negative base-10 logarithm of the transmittance is linear with the liquid turbidity (i.e., concentration of undissolved solids in liquid). Thus, to validate our transmittance estimation, we measured the turbidity of a series of liquids, and then estimated the transmittance values of these liquids using our image-based method.

Our algorithm for image-based liquid transmittance estimation is as follows. Given a segmented liquid region R, let the observed liquid intensity be I_c and the background light intensity be I_b. The transmittance T of the region R is then given by

$$T = \text{median}\{I_c(x,y)/I_b(x,y) : (x,y) \in R\} \quad (4)$$

where median is the operator to find the median value of a set of numbers.

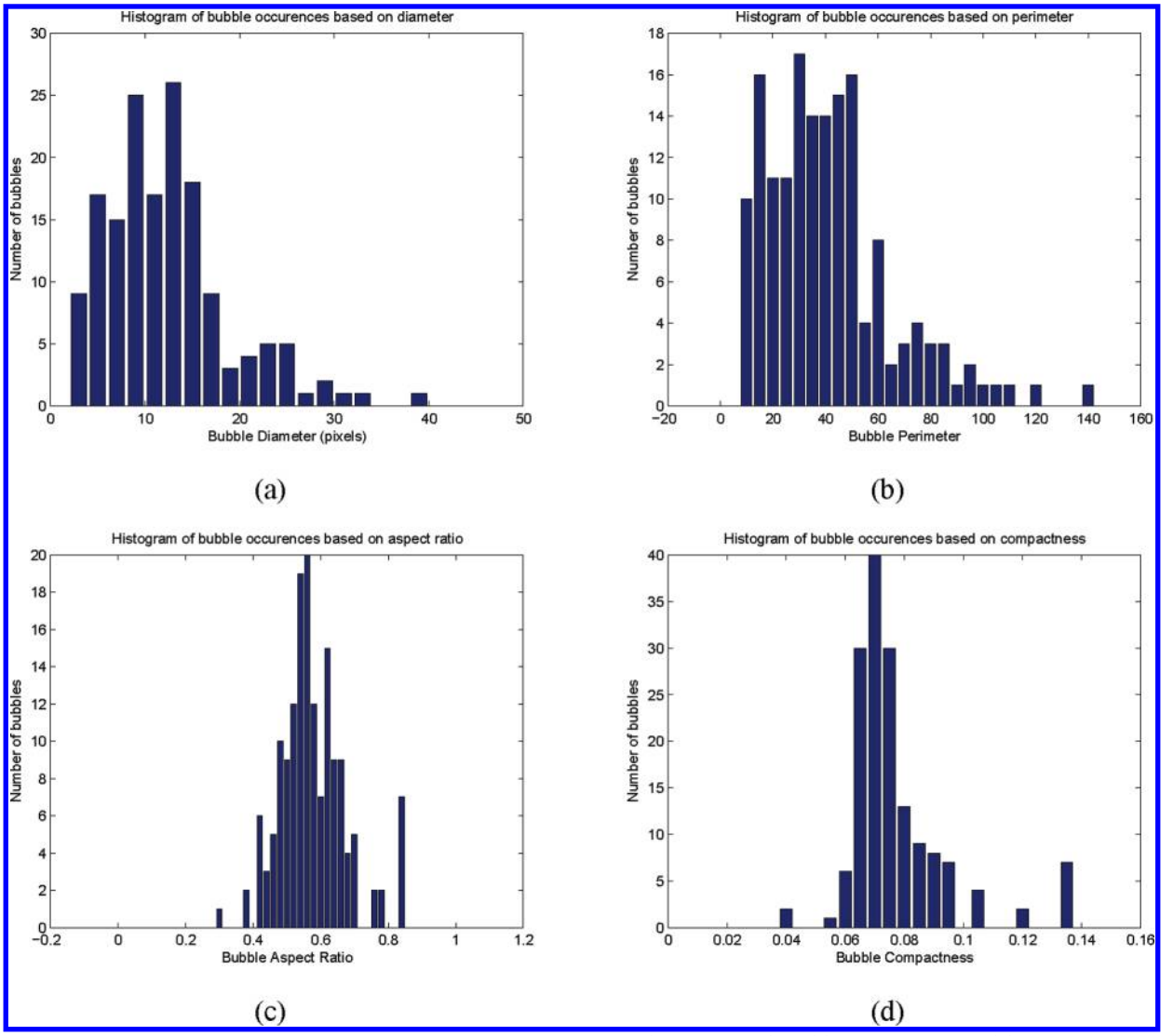

Figure 10. Foam characterization for the foam image in Figure 9: Distributions (or histograms) of (a) bubble diameter, (b) bubble perimeter, (c) bubble aspect ratio, (d) bubble compactness.

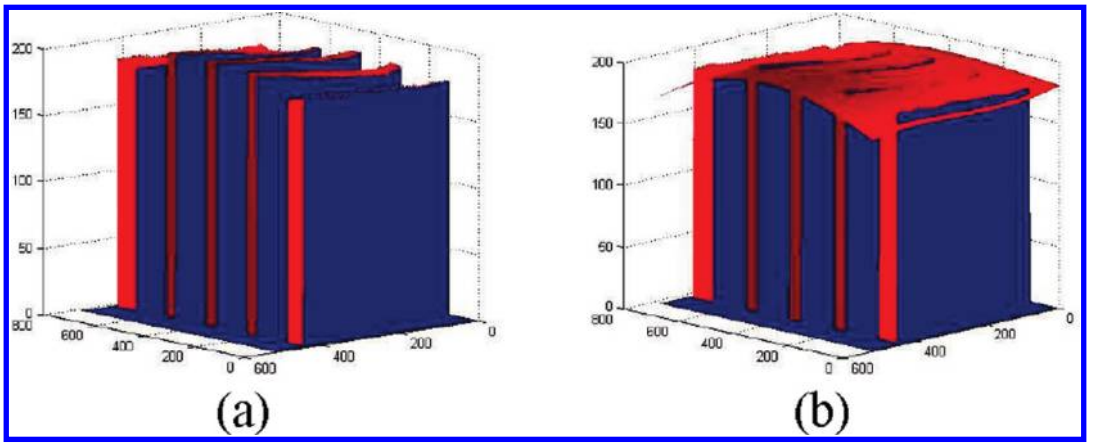

Figure 11. Polynomial surface fitting to estimate background light intensity: (a) Original light intensity in unoccluded areas between tubes, (b) interpolated light intensity surface over the entire image domain.

In eq 4, one can obtain the observed liquid intensity I_c directly from the image intensity in region R. One needs to estimate the background light intensity, I_b, based on image intensity in areas not occluded by the tube and liquid. Because the background

dx.doi.org/10.1021/ie1017833 |*Ind. Eng. Chem. Res.* 2011, 50, 6071–6081

light can be uneven across the image, we used a bicubic polynomial surface fitting technique to estimate the spatially varying background light intensity map. More specifically, let the unoccluded background regions (e.g., between tubes) be denoted R_{light}. Figure 11a shows the image intensity I_b (Z axis) as a function of pixel location (x,y) (X and Y axes) in R_{light}. We applied bicubic surface fitting to interpolate the function over the entire image domain

$$I_b(x,y) = \sum_{i=0}^{3}\sum_{j=0}^{3} a_{ij}x^i y^j \quad (5)$$

This interpolation problem consists of determining the 16 coefficients a_{ij}, and its least-squares solution can be found by using known function values for all pixels $(x,y) \in R_{light}$. Figure 11b shows the interpolated background light intensity I_b both within and between tubes.

In our experiments, we estimated the image-based liquid transmittance in RGB (red, green, blue) color space and computed the transmittance value for each channel separately, represented as T_r, T_g, and T_b, respectively. Then, we combined the three transmittance values to get a single transmittance output T as follows

$$T = \sqrt{\frac{T_r^2 + T_g^2 + T_b^2}{3}} \quad (6)$$

Figure 12 shows the estimated transmittance values of different color channels for several liquid layers. The numbers on top of the images indicate the combined transmittance values T. The relationship between the measured turbidity and the estimated liquid transmittance is shown in Figure 13, which nicely follows the Lambert−Beer law.

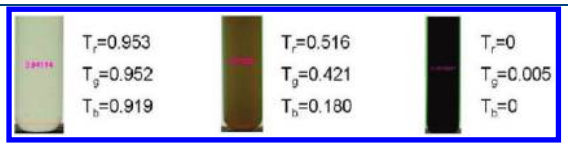

Figure 12. Estimated transmittance values (as defined in eq 6) for several liquids using our image-based method. The transmittance values, from left to right, are 0.9411, 0.3938, and 0.0017.

Because of the known relationship between liquid transmittance and turbidity (Figure 13), image-based estimation of the liquid turbidity can be achieved by estimating transmittance. This method has the potential to provide a more cost-effective and efficient alternative to traditional methods of measuring turbidity.

4. DISCUSSION AND CONCLUSIONS

The method presented in this work uses advanced image segmentation and analysis algorithms to process images of liquid and foam mixtures and perform foam and liquid characterization. Our main contributions include foam type classification using local entropy texture features and the subsequent foam-type-specific bubble segmentation. Our algorithms can segment both loose foam bubbles and densely packed small bubbles. The proposed method is fully automated and enables efficient quantification of important foam and liquid properties based on image information; in particular, our system is able to provide quantitative measures on the texture and color of foaming solutions by calculating bubble size distribution and estimating liquid/foam transmittance.

The foam and liquid characterization system that we built based on this framework is now being used routinely in an industrial laboratory setting. It can process images in a pipeline, performing tube segmentation, liquid and foam layer segmentation, bubble segmentation, and statistical characterization, as well as liquid/foam transmittance estimation. Challenges remain, however, in how to quantify more complex variables such as contact angles at liquid−air and liquid−solid interfaces and bubble rising velocity. Addressing these challenges will require very precise bubble boundary delineation, as well as robust tracking of bubbles in video sequences. Furthermore, three-dimensional characterization could be an extension that provides better accuracy in the presence of occluded bubbles.

AUTHOR INFORMATION

Corresponding Author

*E-mail: xih206@lehigh.edu (X.H.), esmaila@airproducts.com (A.E.).

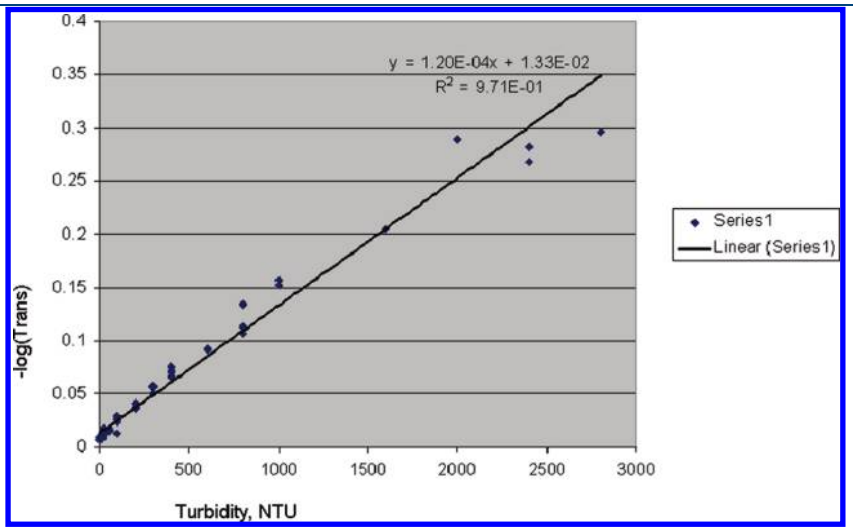

Figure 13. Linear relationship between turbidity and negative base-10 logarithm of transmittance.

■ ACKNOWLEDGMENT

The authors thank Air Products and Chemicals, Inc., for providing data and support for this work. This work was also partially supported by a grant from the Pennsylvania Infrastructure Technology Alliance (PITA).

■ REFERENCES

(1) Heller, J. P.; Kuntamukkula, M. S. Critical review of the foam rheology literature. *Ind. Eng. Chem. Res.* **1987**, *13* (6), 318–325.

(2) Herzhaft, B. Rheology of Aqueous Foams: A Literature Review of Some Experimental Works. *Oil Gas Sci. Technol.* **1999**, *54* (5), 587–596.

(3) Kraynik, A. M. Foam flows. *Annu. Rev. Fluid Mech.* **1988**, *20* (1), 325–357.

(4) Hirschmann, B.; Schönbacher, T.; Temel, A. A New Solvent-Free Defoamer/Deaerator. *Paints Coat. Ind.* **2011**, *27* (1), 36–38.

(5) Semmler, H.; Heilen, W. Elimination and Prevention of Microfoam. *Eur. Coat. J.* **2000**, *6*, 710.

(6) O'Neil, V.; Zeng, J.; Perry, D. New Silicone Foam-Control Agents for Waterborne Coatings. *Paints Coat. Ind.* **2003**, *19* (10).

(7) Capo, J.; Yu, M.; Miska, S. Z.; Takach, N.; Ahmed, R. Cuttings Transport With Aqueous Foam at Intermediate-Inclined Wells. *SPE Drill & Compl* **2006**, *21* (2), 99–107.

(8) Nunez, E.; Chirinos, J.; Villar, R.; Desbiens, A.; Duchesne, C. Predictive Control of Froth Depth and Air Hold-Up in a Pilot Flotation Column. In *Proceedings of International Symposium on Application of Computers and Operations Research in the Mineral Industry (APCOM)*; Magri, E. J., Ed.; Santiago, Chile, 2007; pp 517−524.

(9) Höhler, R.; Cohen-Addad, S. Rheology of liquid foam. *J. Phys.: Condens. Matter* **2005**, *17*, 1041–1070.

(10) Thomas, P. D.; Darton, R. C.; Whalley, P. B. Liquid foam structure analysis by visible light tomography. *Chem. Eng. J.* **1995**, *56* (3), 187–192.

(11) Bailey, M.; Gomez, C. O.; Finch, J. A. Development and application of an image analysis method for wide bubble size distributions. *Miner. Eng.* **2005**, *18* (12), 1214–1221.

(12) Leifer, I.; Leeuw, G. D.; Cohen, L. H. Optical Measurement of Bubbles: System Design and Application. *J. Atmos. Oceanic Technol.* **2003**, *20* (9), 1317–1332.

(13) Bergeron, V.; Walstra, P. Foams. *Fundam. Interface Colloid Sci.* **2005**, *5*, 7–22.

(14) Citir, C.; Aktas, Z.; Berber, R. Off-line image analysis for froth flotation of coal. *Comput. Chem. Eng.* **2004**, *28* (5), 625–632.

(15) Malcolma, A. A.; Leong, H. Y.; Spowage, A. C.; Shacklock, A. P. Image segmentation and analysis for porosity measurement. *J. Mater. Process. Technol.* **2007**, *192*, 391–396.

(16) Hepworth, N. J.; Hammond, J. R. M.; Varley, J. Novel application of computer vision to determine bubble size distributions in beer. *J. Food Eng.* **2004**, *61* (1), 119–124.

(17) Sarker, D. K.; Bertrand, D.; Chtioui, Y; Popineau, Y. Characterisation of foam properties using image analysis. *J. Text. Stud.* **2007**, *29*, 15–42.

(18) Salvo, L.; Cloetens, P.; Maire, E.; Zabler, S.; Blandin, J. J.; Buffiere, J. Y.; Ludwig, W.; Boller, E.; Bellet, D.; Josserond, C. X-ray micro-tomography an attractive characterisation technique in materials science. *Nucl. Instrum. Methods Phys. Res.* **2003**, *200*, 273–286.

(19) Hasanen, A.; Orivuori, P.; Aittamaa, J. Measurements of local bubble size distributions from various flexible membrane diffusers. *Chem. Eng. Process.* **2006**, *45* (4), 291–302.

(20) Rami-shojaei, S.; Vachier, C.; Schmitt, C. Automatic analysis of 2D foam sequences: Application to the characterization of aqueous proteins foams stability. *Image Vision Comput.* **2009**, *27* (6), 609–622.

(21) Zabulis, X.; Papara, M.; Chatziargyriou, A.; Karapantsios, T. D. Detection of densely dispersed spherical bubbles in digital images based on a template matching technique: Application to wet foams. *Colloids Surf. A* **2007**, *309* (1−3), 96–106.

(22) Cheng, D.; Burkhardt, H.; Freiburg, G. Bubble tracking in image sequences. *Int. J. Therm. Sci.* **2003**, *42* (7), 674–665.

(23) Kass, M.; Witkin, A.; Terzopoulos, D. Snakes: Active contour models. *Int. J. Comput. Vision* **1988**, *1* (4), 321–331.

(24) Vincent, L.; Soille, P. Watersheds in digital spaces: An efficient algorithm based on immersion simulations. *IEEE Trans. Pattern Anal. Mach. Intell.* **1991**, *13* (6), 583–598.

(25) Wagner, B.; Dinges, A.; Muller, P.; Haase, G. Parallel Volume Image Segmentation with Watershed Transformation. In *Proceedings of the 16th Scandinavian Conference on Image Analysis (SCIA)*; Salberg, A.-B., Hardeberg, J. Y., Jenssen, R., Eds.; Springer, Lecture Notes in Computer Science (LNCS), Volume 5575, 2009; pp 420−429.

(26) Canny, J. F. A computational approach to edge detection. *IEEE Trans. Pattern Anal. Mach. Intell.* **1986**, *8* (6), 679–698.

(27) Hartigan, J. A.; Wong, M. A. A K-Means Clustering Algorithm. *Appl. Stat.* **1979**, *28*, 100–108.

(28) Shannon, C. E. A mathematical theory of communication. *ACM SIGMOBILE Mobile Comput. Commun. Rev.* **2001**, *5* (1), 3–55.

(29) Althouse, M. L. G.; Chang, C. I. Image segmentation by local entropy methods. In *Proceedings of the IEEE International Conference on Image Processing*; IEEE Computer Society, Washington, DC, 1995; Vol. 3, pp 61−64.

(30) Bakhtiari, A. S.; Shirazi, A. A. B.; Zahmati, A. S. An Efficient Segmentation Method Based on Local Entropy Characteristics of Iris Biometrics. *Int. J. Biol. Life Sci.* **2006**, *2* (3), 195–199.

(31) Fisher, R.; Perkins, S.; Walker, A.; Wolfart, E. Connected Component Labeling, http://homepages.inf.ed.ac.uk/rbf/HIPR2/label.htm (accessed April 3, 2011), 2003.